Nonlinear interaction between wave, breakwater and its loose seabed foundation: A small-scale case

Jianhong Ye [a], Yan Zhang [b,c,*], Ren Wang [a], Changqi Zhu [a]

[a] State Key Laboratory of Geomechanics and Geotechnical Engineering, Institute of Rock and Soil Mechanics, Chinese Academy of Sciences, Wuhan 430071, China
[b] School of Civil and Environment Engineering, University of Science and Technology Beijing, Beijing 10083, China
[c] School of Civil Engineering and Building, Hubei University of Technology, China

ARTICLE INFO

ABSTRACT

In offshore environment, newly deposited quaternary loose sediments widely exist in the world. Sometimes, coastal engineers cannot avoid choosing these natural loose sediments as the foundation of marine structures. Under this situation, the interaction between ocean wave, marine structures and their loose sand foundation, and the wave-induced pore pressure built-up in loose seabed foundation are the key factors in which coastal engineers would most concern. In this study, the nonlinear interaction mechanism between ocean wave, a composite breakwater and its loose elasto-plastic sand bed foundation is investigated by utilizing a semi-coupled numerical model FSSI-CAS 2D. In the coupled numerical model FSSI-CAS 2D, VARANS equation for wave model, and dynamic Biot's equation for soil model are used for the governing equations. The advanced and excellent elasto-plastic constitutive model PZIII proposed by Pastor et al. (1990) is adopted to describe the nonlinear dynamic behavior of loose sand soil under cyclic wave loading. Taking the parameters of Neveda sand determined in the VELACS project funded by NSF as the property parameters for the loose sand bed, a small-scale computational case like the experimental set-up in Mostafa et al. (1999) is taken as a representative case to investigate the wave-structure-loose seabed foundation interaction mechanism. The numerical results indicate that the pore pressure in loose seabed foundation builts up significantly, and the marine structure subsides and tilts under wave loading. The loose sand bed becomes denser and denser due to soil compaction. Parametric studies show that both the wave characteristics and the soil properties can affect the built-up of residual pore pressure in loose seabed foundation.

© 2014 Elsevier Ltd. All rights reserved.

1. Introduction

In recent 20 years, a great number of marine structures, such as breakwater, pipeline, turbine and oil-platform etc., are widely constructed in offshore area to protect coastline or port from erosion and damage, transport fluid (petroleum, natural gas or flesh water), harvest green energy and extract crude oil from seabed. However, these marine structures are vulnerable to the wave-induced liquefaction in their seabed foundation due to the wave-induced excessive excess pore pressure. Some failure examples of breakwater have been reported in previous literature (Harlow, 1980; Zen et al., 1985; Silvester and Hsu, 1989; Lundgren et al., 1989; Sorenson, 1992; Oumeraci, 1994; Franco, 1994; Zhang and Ge, 1996; Guillen, 2008). The main reason for the failure of breakwater built on porous seabed in offshore area could

be attributed to the lack of good understanding of the wave–seabed–structure interaction by coastal engineers involved in the design and maintenance of marine structures.

Two types of seabed soil are widely distributed in offshore area in the world. They are dense sand soil and loose sand soil. Under dynamic loading, the soil particles in dense sand soil seabed would not rearrange their relative position. The soil compaction is difficult to occur. The deformation of dense sand soil is only recoverable if the loading is relatively small. Therefore, the dense sand soil seabed can be regarded as an elastic medium. However, it is worth to mention that the elasticity or elasto-plasticity is a relative conception, because the dilatancy could still occur in dense sand if the magnitude of applied force increasing greatly. Therefore, the elasticity or elasto-plasticity of sand soil is not only dependent on its dense state, but also dependent on the magnitude of applied force.

The newly deposited quaternary loose sand soil in offshore area is a typical elasto-plastic soil. Normally, an elasto-plastic soil has

* Corresponding author.
  E-mail address: yanzhang2009@gmail.com (Y. Zhang).

small value of relative density D_r, S and P wave speed; and has low value of SPT (Standard Penetration Test). Its bearing capacity is generally weak, and it is very easy to liquefy under cyclic loading. Under dynamic loading, such as seismic or wave loading, the soil particles of elasto-plastic soil are rearranged automatically to reach a potential optimal arrangement (more densely), leading to the compaction of soil and the pore pressure build up. After long-term dynamic loading, soil particles of elasto-plastic seabed soil tend to contact with each other more densely, reaching an optimum status. The relative density D_r, S and P wave speed become larger and larger; and SPT value becomes greater. Finally, soil compaction due to plastic volumetric deformation is unlikely to occur again under dynamic loading. Under such situation, the seabed soil becomes elastic porous medium. Therefore, elastic dense seabed floor in natural offshore environment comes from loose deposited soil under long-term wave and/or seismic loading.

Corresponding to the two types of seabed floor, there are two types of response and liquefaction mechanism under wave loading: transient liquefaction in elastic seabed and residual liquefaction in elasto-plastic seabed. The transient liquefaction can only occur in elastic seabed due to the phase lag of the wave-induced pore pressure in elastic seabed. It normally appears repeatedly under wave trough, and mainly depends on the permeability and saturation of seabed soil (Ye, 2012a). Residual liquefaction only can occur in loose seabed due to the pore pressure build up resulting from the compaction of soil under cyclic wave loading. The residual liquefaction is the main risk for the stability of marine structures built on a loose seabed foundation. Two types of liquefaction both have been observed in some laboratory tests and/or fields (Zen and Yamazaki, 1990; Choudhury et al., 2006; Mory et al., 2007; Sumer et al., 2010; Teh et al., 2003; Tzang et al., 2011; Sassa et al., 2006; Sassa and Sekiguchi, 1999).

A great number of investigation have been conducted for the problems of wave–elastic seabed interaction, and the problem of wave–elastic seabed–marine structure interaction so far. The research methods include uncoupled analytical solutions (Hsu and Jeng, 1994; Zhou et al., 2011), coupled analytical solutions (Lee and Lan, 2002; Lee et al., 2002), uncoupled numerical models (Jeng et al., 2001; Ulker et al., 2010), and coupled numerical models (Mizutani et al., 1998; Mostafa et al., 1999; Ye et al., 2013). More detailed literature review on the wave-induced dynamics of elastic seabed, and wave-elastic seabed interaction can be found in Ye, J.H. (2012). However, only few investigation on the wave-induced dynamics of elasto-plastic seabed floor is available at present. Some experimental tests, such as wave flume test (Teh et al., 2003) and geotechnical centrifuge test (Sassa and Sekiguchi, 1999) have been conducted in laboratory to investigate the interaction mechanism between wave and loose sand bed, or wave, breakwater and its loose sand bed. Besides, some uncoupled analytical solutions were proposed to predict the pore pressure build-up in elasto-plastic sand bed under wave loading (Rahman and Jaber, 1986; Cheng et al., 2001; Sumer et al., 2011). In their solutions, a source term function was added to Biot's consolidation equation to approximately describe the mechanism of pore pressure build-up. Actually, these simplified source term functions constructed based on the magnitude of shear stress are unlikely to describe the mechanism accurately. As a result, the predicted pore pressure is not reliable. Basically, they cannot agree adequately with experimental data. Additionally, analytical solutions cannot deal with complex boundary conditions and nonlinear soil constitutive models. A numerical model has natural advantages to deal with complex boundary conditions and soil constitutive models. Some uncoupled numerical models were developed to investigate the wave-induced dynamics, and pore pressure build-up of loose seabed (Li and Jeng, 2008; Dunn et al., 2006; Sassa and Sekiguchi, 2001; Sassa et al., 2001). Among them, Dunn et al. (2006)

adopted the excellent soil constitutive model PZIII (Pastor et al., 1990) to investigate the loose sand–pipeline interaction under regular wave loading. Sassa et al. (2001) proposed a simplified soil constitutive model to simulate the progressive process of residual liquefaction in a loose sand bed under long-tern wave loading. In these numerical models, the effect of marine structures and porous seabed foundation on the wave characteristics, and the effect of wave-induced vibration of marine structures on the dynamics of loose seabed foundation cannot be taken into consideration. To achieve this, an integrated or coupled numerical model is needed.

In this study, the nonlinear interaction mechanism between water wave, composite breakwater and its loose elasto-plastic sand bed foundation is investigated by utilizing a semi-coupled/ integrated numerical model FSSI-CAS 2D (previously known as PORO-WSSI 2D) developed by Ye, J.H. (2012) and Ye et al. (2013). In the integrated/semi-coupled numerical model FSSI-CAS 2D, VAR-ANS equation for wave model, and dynamic Biot's equation for soil model are used for the governing equations. The advanced and excellent elasto-plastic constitutive model PZIII proposed by Pastor et al. (1990) is adopted to describe the dynamic behavior of loose sand soil under cyclic wave loading. It is noted that compressive stress is negative; and soil displacement owning the same direction with the x-, or z-axis is positive in FSSI-CAS 2D.

2. Integrated/coupled numerical model

2.1. Soil model

It has been commonly known that soil is a multi-phase material consisting of soil particles, water and trapped air. In the soil mixture, the soil particles form the skeleton; the water and the air fill the void of skeleton. Therefore, soil is a three-phase porous material, rather than a continuous medium. In this study, the dynamic Biot's equation known as "$u - p$" approximation proposed by Zienkiewicz et al. (1980) are used to govern the dynamic response of porous seabed under wave loading, in which the relative displacements of pore fluid to soil particles are ignored, but the acceleration of the pore water and soil particles are included:

$$\frac{\partial \sigma'_x}{\partial x} + \frac{\partial \tau_{xz}}{\partial z} = -\frac{\partial p}{\partial x} + \rho \frac{\partial^2 u}{\partial t^2}, \tag{1}$$

$$\frac{\partial \tau_{xz}}{\partial x} + \frac{\partial \sigma'_z}{\partial z} + \rho g = -\frac{\partial p}{\partial z} + \rho \frac{\partial^2 w}{\partial t^2}, \tag{2}$$

$$k\nabla^2 p - \gamma_w n\beta \frac{\partial p}{\partial t} + k\rho_f \frac{\partial^2 \epsilon_v}{\partial t^2} = \gamma_w \frac{\partial \epsilon_v}{\partial t}, \tag{3}$$

where (u, w) = the soil displacements in the horizontal and vertical directions, respectively; n = soil porosity; σ'_x and σ'_z = effective normal stresses in the horizontal and vertical directions, respectively; τ_{xz} = shear stress; p = the pore water pressure; $\rho = \rho_f n + \rho_s(1 - n)$ is the average density of porous seabed; ρ_f = the fluid density; ρ_s = solid density; k = Darcy's permeability; g = the gravitational acceleration, γ_ω is unit weight and ϵ_v is the volumetric strain. In Eq. (3), the compressibility of pore fluid (β) and the volume strain (ϵ_v) are defined as

$$\beta = \left(\frac{1}{K_f} + \frac{1 - S_r}{p_{w0}}\right), \tag{4}$$

$$\epsilon_v = \frac{\partial u}{\partial x} + \frac{\partial w}{\partial z}. \tag{5}$$

where S_r = the degree of saturation of seabed, p_{w0} = the absolute static pressure and K_f = the bulk modulus of pore water. Here, it is noted that Eq. (4) describing the compressibility of pore water due

to the unsaturation of soil is only applicable to nearly saturated soil. For the unsaturated soil with saturation less than 50%, it would not hold. However, the range of validity of Eq. (4) is still a research issue. It needs further investigation based on the Soil–Water Characteristics Curve in the framework of unsaturated mechanics.

Under long-term wave loading, loose seabed foundation soil would become denser and denser accompanying the drainage process of pore water. In order to describe this process, the void ratio e of soil is updated in each time step following $e_{n+1} = (1+e_n) \exp(\beta\Delta p + \Delta\epsilon_{vs}) - 1$, where the subscript n stands for nth time step, Δp is the incremental pore pressure, $\Delta\epsilon_{vs}$ is the incremental volume strain of soil.

2.2. Wave model

In this study, the flow field inside and outside of porous media is determined through solving the VARANS equations (Hsu et al., 2002), which are derived by integrating the RANS equations over the control volume. The mass and momentum conservation equations can be expressed as

$$\frac{\partial\langle\overline{u}_{fi}\rangle}{\partial x_i} = 0, \tag{6}$$

$$\frac{\partial\langle\overline{u}_{fi}\rangle}{\partial t} + \frac{\langle\overline{u}_{fj}\rangle}{n(1+c_A)}\frac{\partial\langle\overline{u}_{fi}\rangle}{\partial x_j} = \frac{1}{1+c_A}\left[-\frac{n}{\rho_f}\frac{\partial\langle\overline{p}\rangle^f}{\partial x_i} - \frac{\partial\langle\overline{u'_{fi}u'_{fj}}\rangle}{\partial x_j} + \frac{1}{\rho_f}\frac{\partial\langle\overline{\tau}_{ij}\rangle}{\partial x_j} + ng_i\right]$$
$$-\frac{\langle\overline{u}_i\rangle}{1+c_A}\left[\frac{\alpha(1-n)^2}{n^2 d_{50}^2} + \frac{\beta(1-n)}{n^2 d_{50}}\sqrt{\langle\overline{u}_{f1}\rangle^2 + \langle\overline{u}_{f2}\rangle^2}\right], \tag{7}$$

where u_{fi} is the flow velocity, x_i is the Cartesian coordinate, t is the time, ρ_f is the water density, p is the pressure, τ_{ij} is the viscous stress tensor of mean flow, g_i is the acceleration due to gravity, and n and d_{50} are the porosity and the equivalent mean diameter of the porous material. c_A denotes the added mass coefficient, calculated by $c_A = 0.34(1-n)/n$. $\alpha = 200$ and $\beta = 1.1$ are empirical coefficients associated with the linear and nonlinear drag force, respectively proposed by Liu et al. (1999). More information about the determination of the empirical coefficients α and β can be found in Lin and Karunarathna (2007). Recently, Lara et al. (2011) recommend two nonlinear relations relating the empirical coefficients α and β to the porosity n and mean particle size d_{50}: $\alpha = 4409.22d_{50}$, $\beta = 12.27(n^3/(1-n)^{1.5})d_{50}^{-0.1075}$. It is noted that the VARANS

equation (7) can be degenerated into the RANS equations if the porosity of porous medium $n = 1.0$. It means that the pore is filled with only water, there is no solid matrix. The "⟨normal⟩normal" stands for Darcy's volume averaging operator whose definition can be found in Hsu et al. (2002). The over-bar ("−") represents the ensemble average and the prime ("'") denotes the turbulent fluctuations with respect to the ensemble mean.

The influence of turbulence fluctuations on the mean flow, denoted as $\langle u'_{fi}u'_{fj}\rangle$, is obtained by solving the volume-averaged $k-\epsilon$ turbulence model. In the VARANS equations, the interfacial forces between the fluid and solids have been modeled according to the extended Forchheimer relationship, in which both linear and nonlinear drag forces between pore water and skeleton of porous structures are included in the last term of Eq. (7). More detailed information on the numerical methods and procedures of solving RANS and VARANS equation is available in Lin and Liu (1998) and Hsu et al. (2002).

In this wave model, the internal wave maker proposed by Lin and Liu (1999) is applied to generate the target wave train, in which a mass function is added to the continuity equation. By applying different mass function, various waves could be generated. For example, linear wave, solitary wave, 2nd-order and 5th-order stokes wave, cnoidal wave etc. If the steepness of generated wave reaches up to a certain value, the wave would break when propagating on seabed.

2.3. Integrated method

In the coupling computation, the wave model is responsible for the generation, propagation of wave, and the porous flow in porous structures (seabed, rubble mound and breakwater etc.), and determines the pressure acting on seabed and marine structures. Due to the fact that the VARANS equation is coupled at the interface between fluid domain and porous structures through the pressure and velocity/flux continuity, the pressure and the flow field are continuous in the whole computational domain. At the meantime, the pressure/force acting on seabed and marine structures determined by the wave model is provided to the soil model through a data exchange port developed to calculate the dynamic response of seabed and marine structures, including the displacements, pore pressure and the effective stresses. The coupling process is illustrated in Fig. 1.
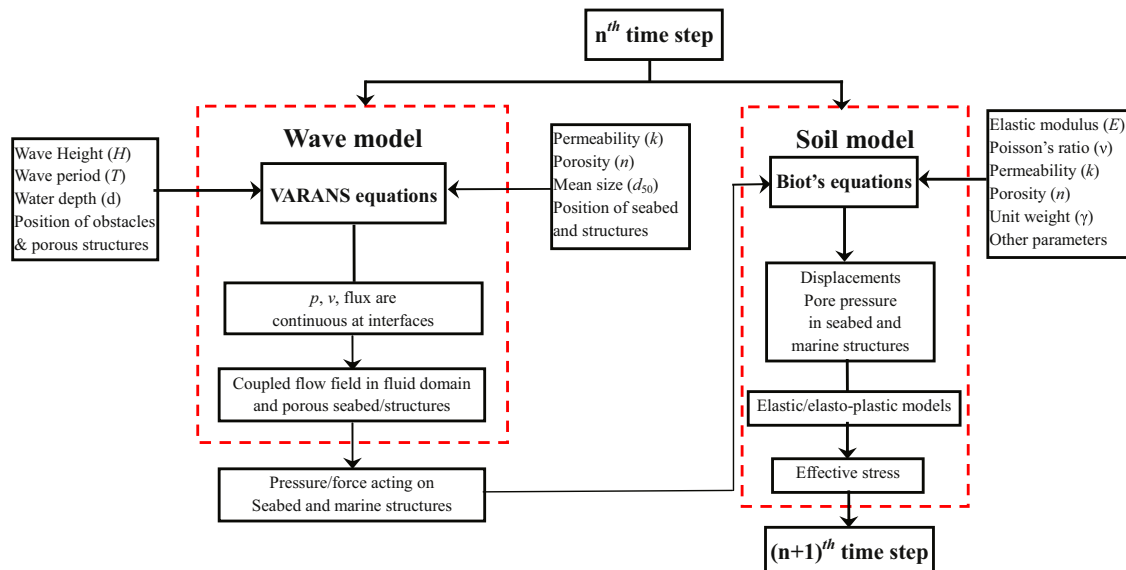

Fig. 1. The coupling process adopted in FSSI-CAS 2D.

It seems that a one way coupling is used in computation as illustrated in Fig. 1. There is no feedback from solid domain to fluid domain. Actually, the coupling between the wave model and soil model can be referred as a semi-coupling process (Ye et al., 2013), because the seabed foundation and rubble mound are considered as a porous medium in the wave model when determining the wave field; the effect of porosity of seabed foundation and rubble mound on wave field has been taken into consideration. Therefore, the flow field in fluid domain and solid domain is continuous at their interfaces. Of course, the pressure and flow velocity of water at interfaces are also certainly continuous. However, the displacement at interfaces is not continuous. From the point view of physics, the wave-induced vibration of marine structures and seabed foundation generally is apparently minor comparing with the wave length. The discontinuity of displacement between fluid domain and solid domain is acceptable. The excellent agreement between numerical results and experimental data in these verification cases further supports this point (Ye et al., 2013). If the displacement continuity on interfaces must be implemented through iterative process (fully coupled), the computation will be very expressive. Additionally, as far as we know, there is no a code so far that can implement the fully coupled computation for wave–seabed–structures interaction problem.

3. Poro-elasto-plastic constitutive model of soil: PZIII

A constitutive model is macroscopic description of the dynamic behavior and deformation of soil under all types of loading. There are normally elastic model and elasto-plastic model widely used in geotechnical engineering computation. Generally, a dense sand soil in offshore environment can be modeled using the elastic model. In the elastic deformation process, the deformation is recoverable; and there is no accumulated plastic strain, namely no swelling and volume contraction. Normally, the elastic dense sand soil processes high shear strength and capacity bearing. It could be an ideal foundation for marine structures. However, dense sand soil in offshore environment is seldom formed. In contrast, newly deposited quaternary loose sand soil is widely existing in the offshore environment in the world. Under dynamic loading, the soil compaction due to uncoverable plastic volumetric deformation occurs in loose sand soil. An elasto-plastic constitutive model must be adopted to model the behavior of loose soil in computation.

Under the generalized plastic theory framework, if an elasto-plastic constitutive model is used for soil in computation, the elasto-plastic matrix D^{ep} should be

$$D_{ijkl}^{ep} = D_{ijkl}^{e} - \frac{D_{ijmn}^{e} m_{mn} n_{st} D_{stkl}^{e}}{H_{L/U} + n_{st} D_{stkl}^{e} m_{kl}} \tag{8}$$

in which D_{ijkl}^{e} is the tensor form of elastic matrix D. $H_{L/U}$ is the plastic modulus at loading or unloading stage. m_{mn} is the plastic flow direction tensor, n_{st} is the loading or unloading direction tensor. The above two direction tensors are formulated as

$$m_{mn} = \frac{\left(\frac{\partial g}{\partial \sigma_{mn}'}\right)}{\left\|\frac{\partial g}{\partial \sigma_{mn}'}\right\|} \quad \text{and} \quad n_{st} = \frac{\left(\frac{\partial f}{\partial \sigma_{st}'}\right)}{\left\|\frac{\partial f}{\partial \sigma_{st}'}\right\|} \tag{9}$$

$\|\partial g/\partial\sigma_{mn}'\|$ and $\|\partial f/\partial\sigma_{st}'\|$ represent the norm of the tensor $\partial g/\partial\sigma_{ij}'$ and $\partial f/\partial\sigma_{ij}'$, respectively. f and g are the yield surface function and plastic potential surface function in stress space, respectively. If the same function is adopted for both yield surface f and plastic potential surface g, then associated flow rule will be applied, otherwise, non-associated flow rule will be applied. In this study, the elasto-plastic constitutive model PZIII (Pastor–Zienkiewicz Mark-III) proposed by Pastor et al. (1990) based on the generalised plastic theory, is adopted to describe the mechanical behavior of loose sandy seabed foundation. In PZIII, the yield surface function f, plastic potential surface function g are respectively defined as

$$f = q' - M_f p' \left(1 + \frac{1}{\alpha_f}\right)\left[1 + \left(\frac{p'}{p_f'}\right)^{\alpha_f}\right] = 0 \tag{10}$$

$$g = q' - M_g p' \left(1 + \frac{1}{\alpha_g}\right)\left[1 + \left(\frac{p'}{p_g'}\right)^{\alpha_g}\right] = 0 \tag{11}$$

The plastic modulus at loading and unloading stage is defined as

$$H_L = H_0 p'\left(1 - \frac{q'/p'}{\eta_f}\right)^4\left[1 - \frac{q'/p'}{M_g} + \beta_0\beta_1\exp(-\beta_0\xi)\right]\left(\frac{q/p'}{\eta_{max}}\right)^{-\gamma_{DM}} \tag{12}$$

$$H_U = \begin{cases} H_{u0}\left(\frac{M_g}{\eta_u}\right)^{\gamma_u} & \text{for}|\frac{M_g}{\eta_u}| > 1 \\ H_{u0} & \text{for}|\frac{M_g}{\eta_u}| \le 1 \end{cases} \tag{13}$$

where p' and q' are the mean effective stress and deviatoric stress, respectively, defined as $p' = \frac{1}{3}(\sigma_{11}' + \sigma_{22}' + \sigma_{33}')$, and $q' = \sqrt{(\sigma_{11}' - \sigma_{22}')^2 + (\sigma_{11}' - \sigma_{33}')^2 + (\sigma_{22}' - \sigma_{33}')^2 + 6(\sigma_{12}^2 + \sigma_{23}^2 + \sigma_{31}^2)}/3$. M_f, M_g, H_0, H_{u0}, η_u, η_{max}, α_f, α_g, β_0, β_1 and γ_u and γ_{DM} are the parameters describing the property of sandy soil. For simplicity, the definition of these parameters can be referred to Pastor et al. (1990) and Zienkiewicz et al. (1999). A smoothed Mohr–Coulomb criterion is adopted to generalize the critical state line (CSL) to three dimensional stress space:

$$M_g = \frac{6\sin\phi}{3 - \sin\phi\sin3\theta'}, \tag{14}$$

in which θ' is Lode's angle, ϕ is the residual internal frictional angle of sand obtained when $\theta' = 30°$ in triaxial compression test.

PZIII is an excellent constitutive model to describe the behaviors of sandy soil. Its reliability has been validated by a series of laboratory tests involving monotonic and cyclic loading (Zienkiewicz et al., 1999). This model is one of the heritages of Olek Zienkiewicz (Pastor et al., 2011).

4. Verification of coupled numerical model

The validity and reliability of the developed semi-coupled numerical model FSSI-CAS 2D have been widely verified by Ye, J.H. (2012). By adopting the analytical solution proposed by Hsu and Jeng (1994), and a series of laboratory wave flume tests conducted by Lu (2005) for regular wave and cnoidal wave, Tsai and Lee (1995) for standing wave, Mizutani et al. (1998) for submerged breakwater, and Mostafa et al. (1999) for composite breakwater, the developed semi-coupled numerical model FSSI-CAS 2D was used to predict the dynamic response of elastic seabed foundation and/or breakwater. The good agreement between the predicted numerical results and the corresponding experimental data indicates that FSSI-CAS 2D is a highly reliable for the problem of Wave–Elastic seabed–Structure Interaction. Furthermore, the validity and reliability of FSSI-CAS 2D for the problem of Wave–Elastoplastic seabed Interaction is also verified by a wave flume test (Teh et al., 2003) and a geotechnical centrifuge test (Sassa and Sekiguchi, 1999). More detailed information about the verification work can be found in Ye, J.H. (2012); and related works have been published in Jeng et al. (2013) and Ye et al. (2013).

5. Analysis of wave–breakwater–elastoplastic seabed interaction

In this section, we take a small scale case (see Fig. 2) like the experimental set-up in Mostafa et al. (1999) as an example to investigate the problem of wave–breakwater–elastoplastic seabed interaction mechanism. In this small-scale case shown in Fig. 2, a composite breakwater consisting of a rubble mound and gravity caisson is constructed on the loose sand bed. The total length and height of the loose sand bed are 3.6 m and 0.19 m, respectively. The PZIII model is an advanced, but also a complex constitutive model. A series of property parameters of soil are needed in computation. In this study, what we focus on is the wave–breakwater–elastoplastic seabed interaction mechanism, rather than determining these property parameters needed in PZIII. Here, the property parameters of Nevada dense sand for PZIII are used for the sand bed in this computational case. These parameters were determined by Zienkiewicz et al. (1999) through a series of dependent laboratory tests available in the VELACS project funded by American National

Science Foundation (NSF). The property parameters used for the loose sand bed foundation, composite breakwater and water wave are listed in Table 1. It is noted here that the permeability and saturation of the loose sand bed is 1.0×10^{-5} m/s, 98% respectively; and the wave height, wave period and water depth is 4 cm, 1.5 s and 40 cm, respectively in a standard computational case. In the computational case for parametric studies, only one of these parameters changes each time, while others keep the same with that in the standard computation case. For the caisson made of impermeable concrete block, its permeability is set as an apparently small value (1.0×10^{-10} m/s). Due to the fact that the rubble mound is composed of gravel with large void ratio, its permeability is set as a great value (1.0×10^{-1} m/s). Additionally, the composite breakwater is modeled utilizing elastic model, because its deformation under wave loading is recoverable.

In this numerical computation for wave–breakwater–elastoplastic seabed interaction, the mesh size in fluid domain is 1–2 cm in the x direction, 0.28–0.38 cm in the z direction. The mesh size in the z direction is about 1/3 to 1/5 of that in the x direction. In the solid domain, the mesh size in the x direction is 2–5 cm, 0.5–2 cm in the
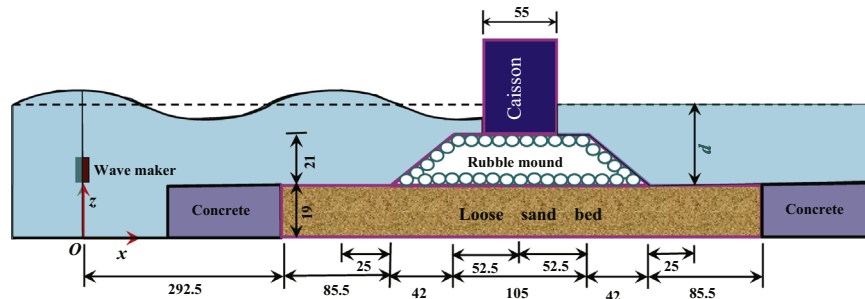

Fig. 2. Set-up and dimension of computational domain similar with the wave flume test conducted by Mostafa et al. (1999).

Table 1
Properties and parameters used for loose seabed foundation, composite breakwater and wave in analysis and parametric study.

Item	Value	Unit
Parameters for PZ3 model (Nevada sand)		
K_{evo}	2000	[kPa]
K_{eso}	2600	[kPa]
p'_0	4	[kPa]
M_g	1.32	–
M_f	1.3	–
α_f	0.45	–
α_g	0.45	–
β_0	4.2	–
β_1	0.2	–
H_0	750	–
H_{U0}	40,000	[kPa]
γ_u	2.0	–
γ_{DM}	4.0	–
Soil characteristics		
permeability	1.0×10^{-2}, 1.0×10^{-5} or 1.0×10^{-7}	[m/s]
Poisson's ratio	0.3333	
Saturation	98	%

	Concrete block caisson	Rubble mound	
Breakwater			
Permeability	1.0×10^{-10}	2.0×10^{-1}	[m/s]
Poisson's ratio	0.25	0.3333	
Saturation	0	99	%
Young's modulus	1.0×10^4	1.0×10^3	[MPa]
Wave characteristics			
Wave height		4, 6	[cm]
Wave period		1.5, 2.0	[s]
Water depth		40, 30	[cm]

z direction, respectively. The horizontal mesh size in fluid and solid domains is less than $L/200$, and $L/40$, respectively (L is wave length). The convergence condition for FSSI-CAS 2D is satisfied (Ye et al., 2013). As shown in Fig. 3, it can be seen that the mesh size in upper sand bed is much more dense than that in lower sand bed. This way could make the numerical results be more clearer to reflect the wave–breakwater–elastoplastic sand bed interaction mechanism.

The following boundary conditions for this computational domain are applied in computation:

(1) The bottom of seabed foundation is treated as rigid and impermeable:

$$u = w = 0 \quad \text{and} \quad \frac{\partial p}{\partial z} = 0 \text{ at } z = 0 \qquad (15)$$

(2) The two lateral sides of seabed are fixed in the x direction:

$$u = 0 \text{ at } x = 2.925 \text{ m} \quad \text{and} \quad x = 6.525 \text{ m} \qquad (16)$$

(3) The surface of seabed, and the outer surface of rubble mound, concrete caisson are applied perpendicularly by hydrostatic pressure, and wave-induced dynamic pressure. The pore pressure is continuous at the interface between seabed, breakwater and water.
(4) There is a upward buoyancy force acting on the bottom of concrete caisson due to its impermeability. This buoyancy force is considered in coupling computation.

5.1. Consolidation of seabed foundation

In the offshore environment, seabed floor generally has experienced the consolidation process under the hydrostatic seawater pressure and self-gravity in the geological history. Additionally, after a breakwater is built on seabed floor, the seabed beneath and near to the composite breakwater will be compressed, and deform
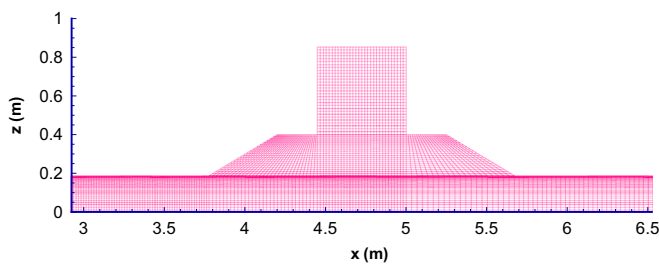

Fig. 3. FEM mesh used in computation for sandy bed and composite breakwater.

under the gravity of breakwater. As a result, at the initial stage, the pore pressure in the seabed beneath marine structures significantly increases. It is called excess pore pressure. As time passing, the excess pore pressure due to the construction of marine structures will gradually dissipate through water drainage. Finally, a new equilibrium state is reached, in which there is no any excess pore pressure in seabed foundation. From the point of view of physics, in order to simulate the interaction between ocean wave, the composite breakwater and its loose seabed foundation, the initial consolidation status of the seabed foundation under hydrostatic pressure and the gravity of the breakwater should be firstly determined. Then, this consolidation status is taken as the initial condition for the followed dynamic analysis.

Fig. 4 demonstrates the pore pressure dissipation in the sand bed ($x = 4.725$ m, $z = 0.1024$ m), and the subsidence of the composite breakwater ($x = 4.725$ m, $z = 0.85$ m) in the process of consolidation. In Fig. 4, it can be seen that the excess pore pressure in the sand bed under the composite breakwater is huge at the initial stage of consolidation. Most of the gravity of the composite breakwater is beared by pore water. As time passing, the excess pore pressure in the sand bed due to the construction of the composite breakwater gradually dissipates. The contact effective stresses between soil particles gradually increase. The loading beared by pore water gradually migrates to soil particles. At the meantime, the composite breakwater subsides downward. Finally, the excess pore pressure disappears completely, only hydrostatic pressure existing in the sand bed.

Fig. 5 illustrates the distribution of effective stresses and pore pressure in the final consolidation status. In Fig. 5, it is found that the horizontal effective stresses σ'_x and σ'_y have a similar distribution in the computational domain. There are two obvious stress concentration zones in the rubble mound. In the upper part of rubble mound, σ'_x and σ'_y are both compressive; while, they are both tensile in the lower part of rubble mound. The magnitude of σ'_x and σ'_y in the sand bed is much less than that in the rubble mound. The distribution of σ'_z indicates that the effect of the composite breakwater on the stress field is significant. In the zone of seabed beneath the composite breakwater, the vertical effective stress σ'_z increases greatly due to the gravity compression of the composite breakwater. However, its range of influence is limited. In the region of seabed away from the composite breakwater, the distribution of σ'_z becomes layered. It is interesting to find that σ'_z is not continuous at the interface between the caisson and the rubble mound. This phenomenon can be attributed to the fact that the upward buoyancy force on the bottom of concrete caisson is considered in computation. The shear stress is mainly concentrated in the rubble mound; and their directions are opposite. Due to the fact that the caisson is impermeable, there is no pore pressure in the concrete caisson. The distribution of pore pressure
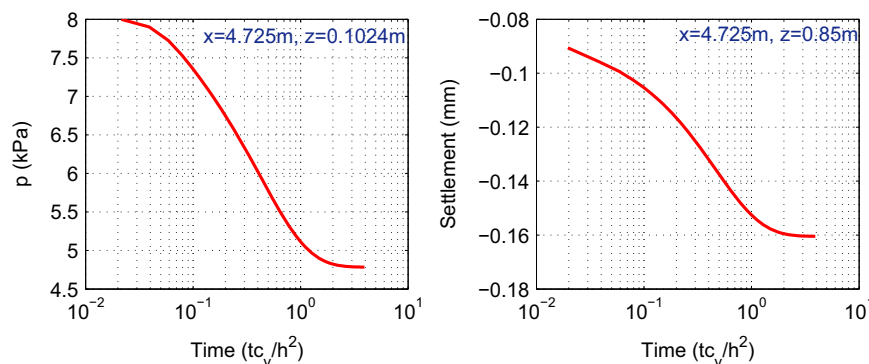

Fig. 4. Pore pressure dissipation in sand bed, and subsidence of breakwater in consolidation process. (Noted: h is the depth of seabed foundation, and c_v is the consolidation coefficient of seabed soil.)
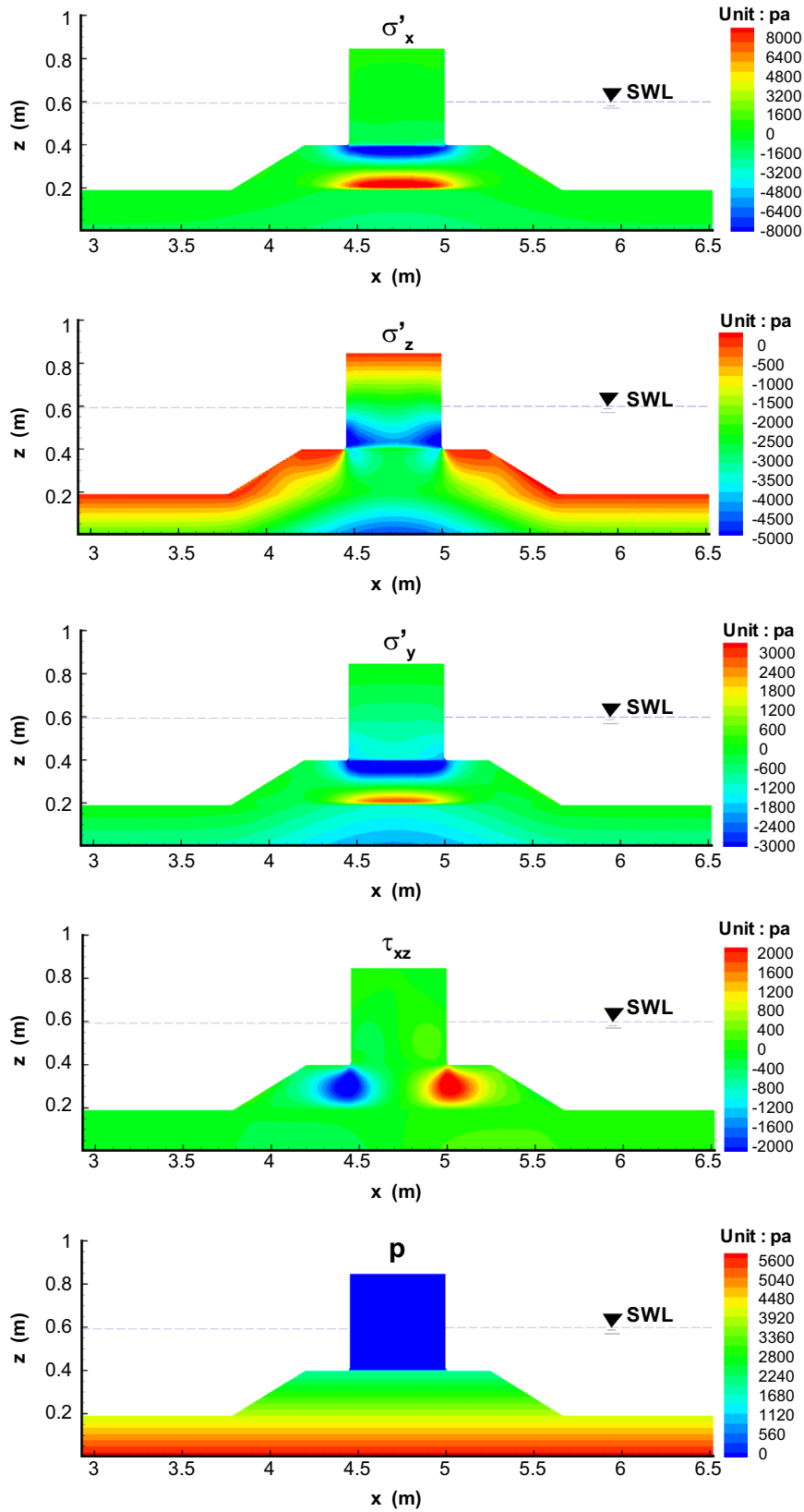
Fig. 5. Distribution of effective stresses σ'_x, σ'_x and τ_{xz}, and pore pressure p in the consolidation status.

in the sand bed and rubble mound is layered. Its magnitude increases linearly with depth.

Fig. 6 shows the distribution of horizontal and vertical displacement u, w in the sand bed and composite breakwater. As shown in Fig. 6, the distribution of displacements is basically symmetrical along x=4.725 m. Under the gravity compression of the composite breakwater, the sand bed under the breakwater moves toward its two lateral sides; and the concrete caisson

Fig. 6. Distribution of horizontal and vertical displacement u, w in the consolidation status.

subsides downward as a whole. In the practice of engineering, the final subsidence of the caisson is mainly dependent on the stiffness and shear strength of seabed foundation. More detailed analysis of consolidation of seabed foundation under hydrostatic pressure and various types of breakwater can be found in Ye et al. (2012), Ye (2012b) and Jeng and Ye (2012).

5.2. Wave field and impact on seabed and breakwater

Taking the above determined consolidation status as the initial condition, the interaction between water wave, composite breakwater and its elastoplastic seabed foundation is investigated. In the standard computational case, the wave characteristics used are wave height=4 cm, wave period=1.5 s, water depth=40 cm. The internal wave maker is located at the position $x = -15$ m, which is far away from the composite breakwater. The distance from the internal wave maker to the breakwater is about 10 times of the wave length, making the water wave becomes more established and stable when arriving at the breakwater. The time step is automatically controlled by the code to satisfy the convergence condition. Fig. 7 illustrates the velocity field, and the surface profile of the water wave at time $t = 50$ s. In the computation for wave motion, the caisson is treated as an impermeable object. The rubble mound and the sand bed are both treated as porous media. The linear and nonlinear drag force between pore water flow and solid matrix are included as shown in Eq. (7). Due to the fact that the flow speed of pore water in the rubble mound and sand bed is relatively small comparing with that in the fluid domain, the velocity vectors in the rubble mound and sand bed look like points. Also due to the shielding effect of the breakwater for wave propagating, the water in the zone locating at the right side of breakwater basically keeps static.

In the interaction process between wave, composite breakwater and its elastoplastic sand bed, the wave continuously applies loading on the sand bed and the composite breakwater. The wave-induced force is the driven source for the caisson vibration, and the pore pressure built-up in the sand bed. Fig. 8 representatively illustrates the wave-induced dynamic pressure on the sand bed at
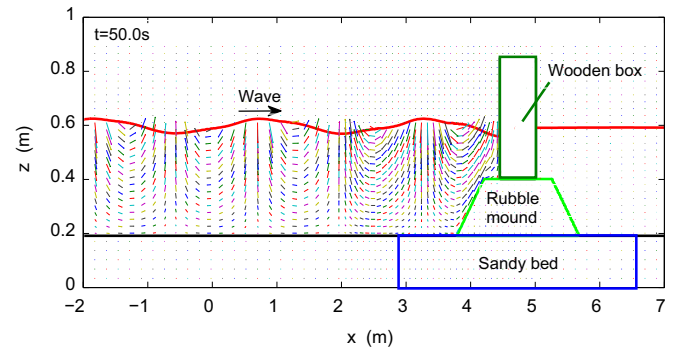

Fig. 7. Velocity field of fluid motion in front of breakwater and in porous seabed at $t = 50$ s.
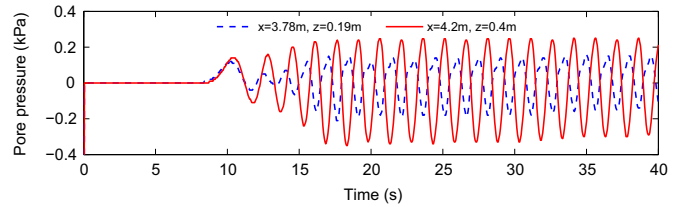

Fig. 8. Wave-induced dynamic pressure acting on the seabed and rubble mound.

$x = 3.78$ m, $z = 0.19$ m and on the rubble mound at $x = 4.2$ m, $z = 0.4$ m. As illustrated in Fig. 8, the wave-induced dynamic pressure on the sand bed and rubble mound is periodic; and the dynamic pressure on the sand bed is significantly less than that on the rubble mound. It is interesting to find that the wave interference between incident wave and reflected wave in front of the composite breakwater becomes stable after three wave periods from the incident wave firstly arriving at the breakwater. Fig. 9 demonstrates the wave-induced impact on the left lateral side of the caisson. As demonstrated in Fig. 9, the hydrostatic pressure is applied before the incident wave arriving. The wave-induced impact acting on the left lateral side of the caisson reaches up

200 N/m. This impact directly drives the caisson vibrating periodically.

5.3. Dynamic response of composite breakwater

Taking the wave-induced pressure acting on the sand bed and on the composite breakwater as the boundary condition, the dynamics of the breakwater and its sand foundation is investigated numerically. The time step is set as $T/50 = 0.03$ s. Fig. 10 illustrates the horizontal and vertical displacements of a typical point on the breakwater (top-left corner of the caisson). As illustrated in Fig. 10, the breakwater vibrates periodically about its original equilibrium position if the seabed foundation is elastic (very dense sand). For the loose sand in this study, the PZIII model is used to describe its dynamical behavior. It can be seen that the breakwater not only vibrates periodically, but also continuously tilts to the left under the long-term wave loading. This tilting can be attributed to the softening of the left side sand bed under wave loading. The loose sand bed always has liquefaction potential due to the pore pressure built-up under wave loading. As we know, liquefied sand will completely lose its shear strength and bearing capacity. When the cumulative amount of tilt excesses a critical value, the breakwater will fail due to collapse. This kind of failure mechanism would be the reason for some failure cases of offshore marine structures in the world.

5.4. Dynamic response of seabed foundation

In the practice of offshore engineering, seabed floor is generally taken as a kind of natural foundation for marine structures. The wave-induced dynamic response of a densely elastic seabed has been comprehensively investigated in previous literature, detailed review can be found in Ye, J.H. (2012). In the offshore environment, newly deposited quaternary loose soil is widely distributed in the world. In the practice of offshore engineering, coastal engineers cannot avoid the situation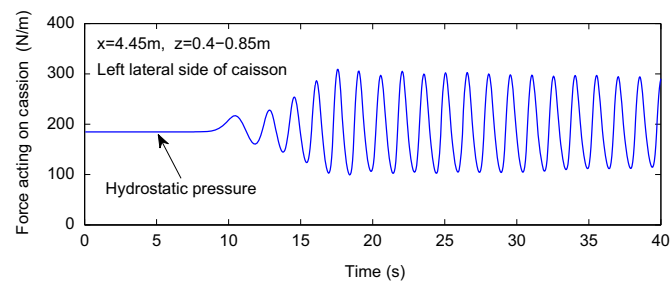 sometimes that they have to choose the loose sand soil seabed as the foundation of marine structures. Under cyclic/periodical wave loading, the soil particles in loose seabed foundation would re-arrange their relative position to a more dense status accompanying a drainage process, making the void ratio decrease. As a result, the pore pressure in loose seabed foundation will built-up, and marine structures built on loose seabed foundation will subside and tilt, even collapse. Therefore, the wave-induced dynamic response of a loose seabed foundation is a key point in the wave–breakwater–elastoplastic seabed foundation interaction mechanism.

The pore pressure and effective stresses at three typical points in the sand bed are recorded in computation. They are located respectively at the position A: $x = 3.78$ m, $z = 0.1694$ m (under the left foot of the rubble mound), B: $x = 4.725$ m, $z = 0.1694$ m (under the middle part of the rubble mound), and C: $x = 5.67$ m, $z = 0.1694$ m (under the right foot of the rubble mound). Figs. 11–13 graphically show the time history curve of the wave-induced pore pressure and effective stresses at the three typical positions. In Fig. 11, it can be seen that the pore pressure at the position A ($x = 3.78$ m, $z = 0.1694$ m) gradually builts up until the time $t = 60$ s. It is indicated that the rate of pore pressure built-up is greater than the rate of pore pressure dissipation. After $t = 60$ s, the pore pressure dissipation is quicker than the pore pressure built-up. As a result, the pore pressure at A ($x = 3.78$ m, $z = 0.1694$ m) decreases. This phenomenon indicates that the cyclic wave loading-induced volume contraction in the loose seabed foundation basically tends to zero after $t = 60$ s. The contact effective stresses σ'_x and σ'_z both decrease at early stage (before $t = 20$ s), and increase at late stage. This trend would be attributed to the fact that the pore pressure built-up make the contact effective stresses between soil particles decrease at early stage; however, the significant downward subsidence of the composite breakwater force the contact effective stresses between soil particles under the foot of the rubble mound increase at late stage, even though the pore pressure continuously built up in the time $t = 20$–60 s. In the interaction process, the shear stress gradually approaches zero. From a conventional perspective, the shear stress should increase when the contact effective stress of soil particles increasing. However, the shear stress at position A ($x = 3.78$ m, $z = 0.1694$ m) continuously decreases. This phenomenon would be closely related to the high nonlinearity of the interaction.

In Fig. 12, the time history curve of pore pressure built-up at the position B ($x = 4.725$ m, $z = 0.1694$ m) is basically the same with that at the position A ($x = 3.78$ m, $z = 0.1694$ m). The maximum excess pore pressure is about 130 Pa, which is less than that at A ($x = 3.78$ m, $z = 0.1694$ m). It is attributed to the fact that the sand soil under the middle part of the rubble mound is not directly applied by wave loading. The volume contraction and the pore pressure built-up in the seabed under the middle part of rubble
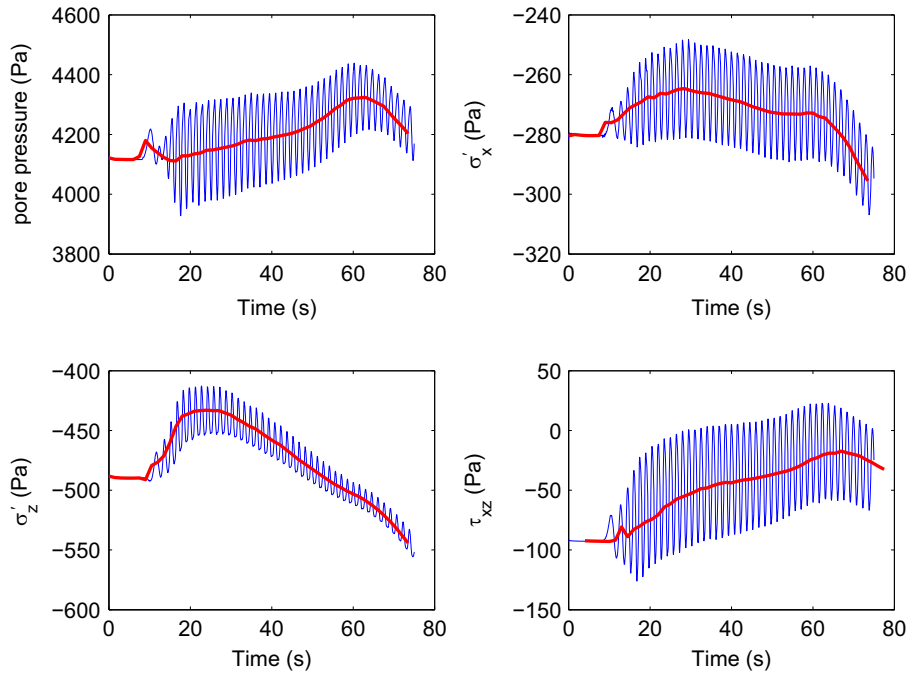

Fig. 9. Wave-induced impact force acting on the left lateral side of caisson.

Fig. 10. Horizontal and vertical displacement of typical point ($x = 4.45$ m, $z = 0.85$ m) on the breakwater.

Fig. 11. Time history curve of wave-induced pore pressure and effective stresses in the sand bed at A ($x=3.78$ m, $z=0.1694$ m), which is under the left foot of the rubble mound.
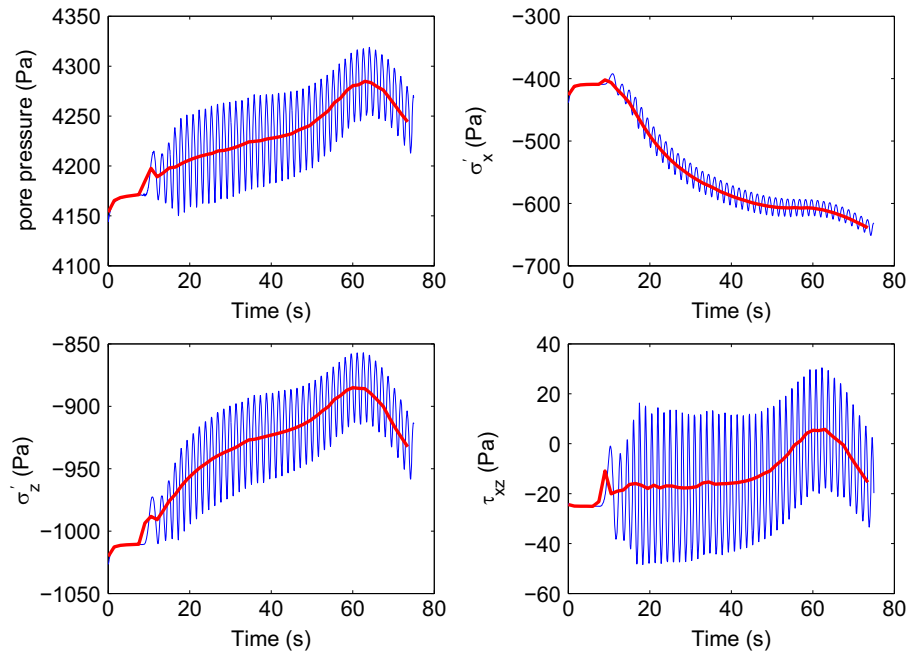

Fig. 12. Time history curve of wave-induced pore pressure and effective stresses in the sand bed at B ($x=4.725$ m, $z=0.1694$ m), which is under the middle part of the rubble mound.

mound are mainly caused by the wave-induced vibration of the composite breakwater. Also because of this reason, the variation of σ'_x at B ($x=4.725$ m, $z=0.1694$ m) is completely different from that at A ($x=3.78$ m, $z=0.1694$ m). σ'_x at B ($x=4.725$ m, $z=0.1694$ m) continuously increases in the whole interaction process.

In Fig. 13, the time history curve of pore pressure built-up at the position C ($x=5.67$ m, $z=0.1694$ m) is also basically the same with that at the two positions mentioned above. The maximum wave-induced excess pore pressure is only 50 Pa. However, the variation of the effective stresses σ'_x and σ'_z at this position appears to be much more complex. This observed result from a reliable

numerical model reflects to some extend that the problem of wave, marine structure and its loose elastic seabed foundation interaction is complex, and highly nonlinear.

In the computation model, the rubble mound is made of large grain size gravel, and the porosity ratio is large. The wave-induced impact acting on the breakwater basically is impossible to make the large gravel to rearrange their relative position; namely there is no volume contraction. Additionally, the great void ratio of the rubble mound makes the dissipation of excess pore pressure is very fast. As a result, the pore pressure in the rubble mound can only vary periodically, see Fig. 14.
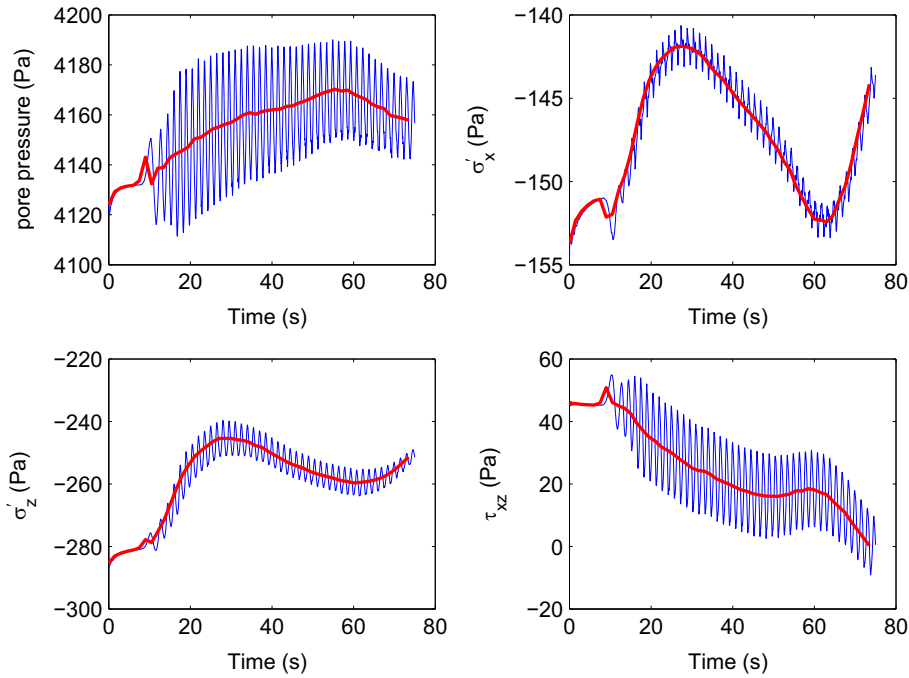
Fig. 13. Time history curve of wave-induced pore pressure and effective stresses in the sand bed at C ($x = 5.67$ m, $z = 0.1694$ m), which is under the right foot of the rubble mound.

The above analysis is based on some specific positions (A–D). The distribution of wave-induced residual pore pressure along the depth of seabed foundation is also an interesting issue. Fig. 15 demonstrates the distribution of wave-induced residual pore pressure along depth at three different positions $x = 3.78$ m, $x = 4.725$ m and $x = 5.67$ m. In Fig. 15, the following conclusions can be observed: (1) the residual pore pressure on the surface of sand bed is always zero, because it is the boundary condition, whenever the time, and wherever it located at. (2) The residual pore pressure increases gradually along depth under long term wave loading in the whole sand bed foundation; however, the residual pore pressure cannot built up infinitely. It is limited by the overburden soil weight, because the sand soil will liquefy once the residual pore pressure overcomes its overburden soil weight at one position. (3) After 33 times wave loading, the residual pore pressure on $x = 3.78$ m (under the left foot of rubble mound) is greatest, while it is smallest on $x = 5.67$ m (under the right foot of rubble mound). It is indicated that the seabed foundation at the left-hand side of the composite breakwater is most affected by the wave loading. The breakwater can effectively block the direct effect of wave for the seabed behind the breakwater. The generation of residual pore pressure in the seabed foundation under the rubble mound and behind the breakwater is mainly attributed to the wave-induced vibration of breakwater, and the diffusion of pore pressure from high pressure zone to low pressure zone.

Fig. 16 demonstrates the distribution of wave-induced vertical effective stress σ'_z and the residual pore pressure in the seabed–breakwater system at time $t = 60$ s. As demonstrated in Fig. 16, the wave-induced dynamic σ'_z and residual pore pressure mainly concentrate in the zone located at the left-hand side of the composite breakwater. The reason for this phenomenon is that the left part of the sand bed is directly applied by wave loading; and the cyclic wave loading and the periodical vibration of the breakwater make the volume contraction of soil in the left part of the sand bed is much faster than that in the right part of the sand bed. Based on the principle of effective stresses, the built-up of pore pressure will make the contact effective stresses between soil particles to decrease. When the effective stresses decrease to zero,

the sand soil becomes liquefied. Therefore, the distribution of vertical effective stress σ'_z in the sand bed is corresponding to the distribution of residual pore pressure. Due to the fact that the caisson is impermeable, and the rubble mound is highly permeable, the residual pore pressure in them cannot built up. The residual pore pressure in the caisson and rubble mound is basically zero, as shown in Fig. 16. There is another interesting phenomenon as shown in Fig. 16. The residual pore pressure in the lower sand bed is much greater than that in the upper sand bed under the long term wave loading. This result observed in Fig. 16 can be attributed to the difference of drainage condition in the sand bed. It is much more difficult to drain out the surface of sand bed for the pore water in lower sand bed. Although the sand bed at the right-hand side of the composite breakwater is not directly applied by the wave loading, the residual pore pressure still exists in the right part of sand bed. The generation of residual pore pressure in the right part of sand bed can be attributed to the periodical vibration of the breakwater, and the diffusion of pressure from high pressure zone to low pressure zone.

As analyzed above, we know that the pore pressure builts up under wave loading in loose sand bed, making the contact effective stresses between soil particles varying in a very complex manner. Stress path in $p' - q'$ coordinates is a useful method to investigate the variation of effective stress status in the sand bed under cyclic wave loading. Fig. 17 illustrates the effective stress path at five representative positions in the elasto-plastic loose sand bed. In Fig. 17, it can be found that the effective stress path in $p' - q'$ coordinates circles along a flat oval if the sand bed is elastic (very dense); however, the effective stress path moves substantially under wave loading for loose elastoplastic sand bed. It is indicated that an unrecoverable interaction process occurs in the loose sand bed under wave loading. From the physical point of view, this unrecoverable process is the compaction of soil, and the subsidence of breakwater. From the stress paths shown in Fig. 17, it is seen that the final effective stress status does not approach the zero stress. It is indicated that the sand bed is far away from the liquefaction state in the interaction process. Another result can be observed in Fig. 17 is that the stress paths move faster in the early

stage; while, they move very slow in the late stage. The reason for this would be that the loose sand bed gradually becomes denser and denser, and harder and harder under the wave loading. The ultimate movement would be the same with that of a dense elastic sand bed, namely circulation along a flat oval.

Under long-term wave loading, the sand bed foundation becomes denser and denser due to the rearrangement of soil particles to a dense state. As a result, the sand bed foundation and the composite breakwater subside downward. Because the soil compaction in the sand bed foundation is not uniform, the breakwater tilts to left side. Fig. 18 illustrates the distribution of the horizontal and vertical displacement in the sandy bed and composite breakwater after time $t/T=50$. In Fig. 18, it is found that the vertical displacement is generally one order (O(1)) of magnitude larger than the horizontal displacement. It is indicated that the downward subsidence is the dominant deformation for the sand bed and the composite breakwater under wave loading. Due to the constraint by the fixed horizontal boundary, the horizontal displacement of seabed soil is apparently small. The subsidence in the left part of the sand bed is much greater than that in the right part. As a result, the composite breakwater tilts to left side. In the sand

bed under the left foot of the rubble mound, the unrecoverable deformation is significant.

5.5. Parametric study

In the above analysis, the Nevada sand with standard parameters ($k=1.0 \times 10^{-5}$ m/s, $S_r=98\%$, $H=4$ cm, $T=1.5$ s, $d=0.4$ m) is used for the loose seabed foundation. It is a question how the parameters affect the pore pressure build-up in the seabed foundation under wave loading. In this section, a parametric study is conducted to investigate the effect of soil properties and wave characteristics on the pore pressure build-up in the seabed foundation. Here, only the line $x=3.78$ m is taken as the representative to demonstrate the effect of parameters.

Fig. 19 demonstrates the distribution of wave-induced residual pore pressure along the line $x=3.78$ m under different wave loading. In Fig. 19, the effect of wave characteristics on the wave-induced residual pore pressure can be observed clearly. It is shown that the water waves in shallow water with large wave height and long wave period make the wave-induced residual pore pressure in loose seabed foundation built up more quickly. The reason for this phenomenon is that the waves in shallow water with large height and long period carry more energy, making the vibration of breakwater is more fierce, and the magnitude of wave-induced cyclic shear stress in seabed foundation is much greater. The above two factors further jointly promote the volume contraction due to the soil particle rearrangement under cyclic shearing and vibration is much faster.

Fig. 20 illustrates the distribution of wave-induced residual pore pressure along the line $x=3.78$ m in the seabed foundation with different saturation or different permeability. In Fig. 20, it can
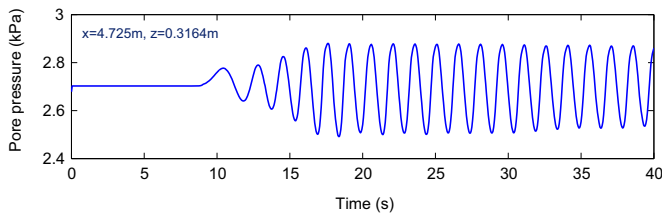

Fig. 14. Time history curve of wave-induced pore pressure at the central point in the rubble mound D ($x=4.75$ m, $z=0.3164$ m).
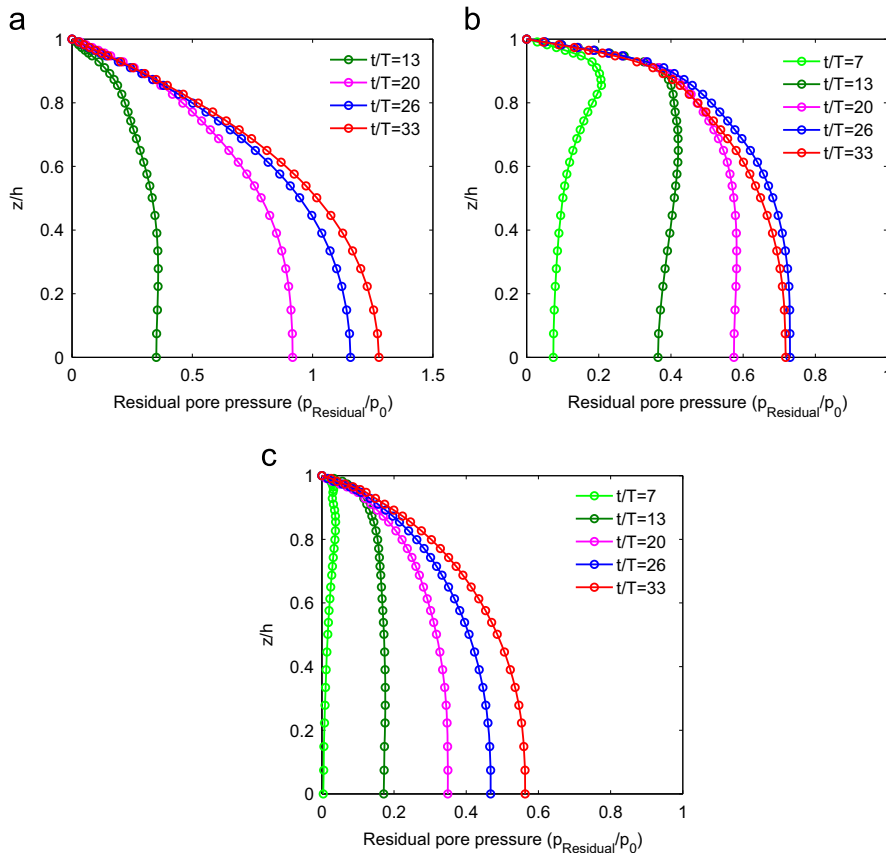

Fig. 15. Distribution of wave-induced residual pore pressure along depth at three different positions in the elasto-plastic sand bed.
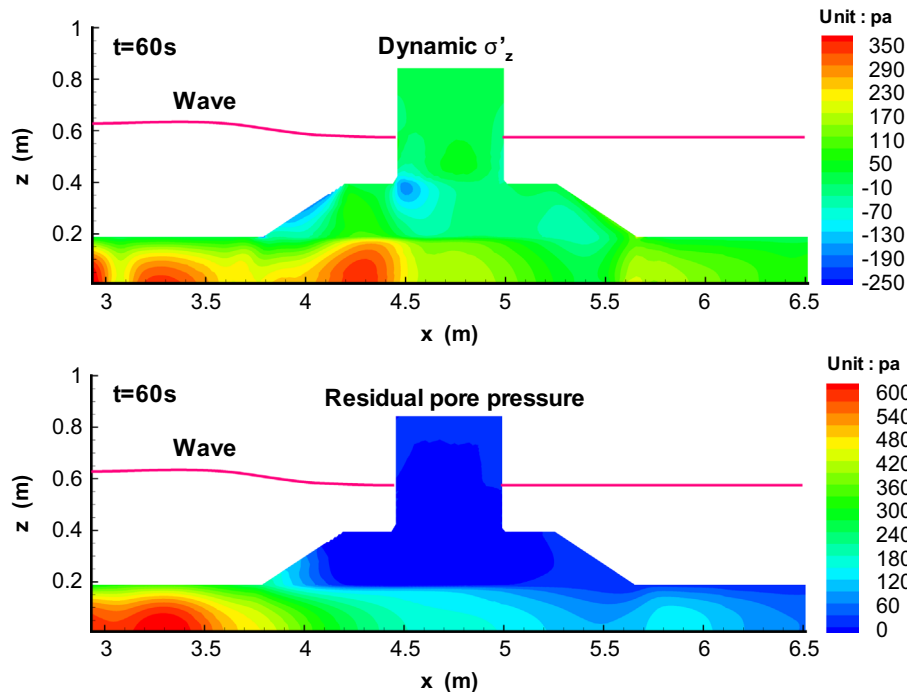
Fig. 16. Wave-induced residual pore pressure and vertical effective stress in the elasto-plastic sand bed at time $t=60$ s. (Noted: compressive stress is negative.)
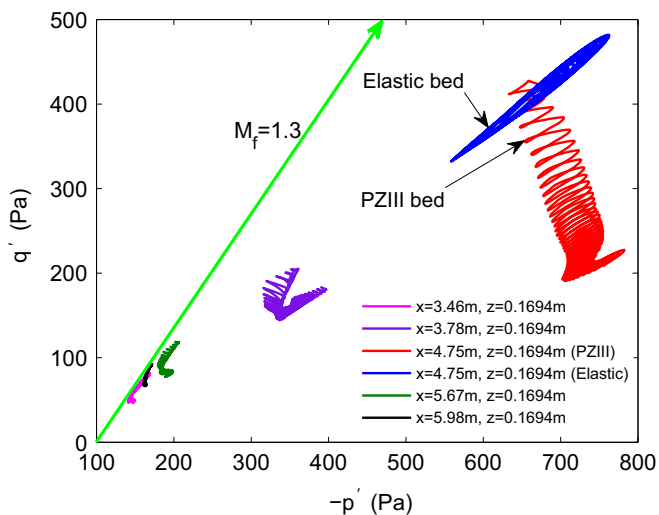

Fig. 17. Effective stress path at five representative positions in the elasto-plastic loose bed.

be seen that the saturated sand bed is much easier to built up the pore pressure under wave loading than the unsaturated sand bed, even though the difference of saturation is only 2%. This phenomenon can be attributed to the fact the compressibility of pore fluid (pore water and trapped air) in unsaturated soil ($S_r = 98\%$) is 100 times of that in saturated soil. Due to the significant compressibility of pore fluid in unsaturated soil, the pore pressure in unsaturated soil is difficult to built up under the same wave loading. In Fig. 20, it is also can be seen that the permeability of soil is the most important factor affecting the pore pressure built-up in sand soil. For the soil with huge permeability, the dissipation of pore pressure is apparently fast. It is basically impossible for the pore pressure to built up in it. For the soil with small permeability, the pore pressure built-up under wave loading is very significant. However, the distribution of the residual pore pressure along depth is a little orderless. The possible reason for the unstable

result when $k=1.0 \times 10^{-7}$ m/s is that the numerical volumetric locking occurs under the nearly undrained condition. Previous investigation proposed the usage of less node of fluid than that of solid in a FEM element to solving this problem. Currently, our soil model cannot handle this type of element. Further work is needed in the future.

6. Conclusion

In this study, the interaction mechanism between water wave, composite breakwater and its loose elasto-plastic sand bed foundation is investigated by adopting a semi-coupled numerical model FSSI-CAS 2D developed by Ye, J.H. (2012) and Ye et al. (2013). In the semi-coupled numerical model FSSI-CAS 2D, VAR-ANS equation for wave model, and dynamic Biot's equation for soil model are used for the governing equations. The advanced and excellent elasto-plastic constitutive model PZIII proposed by Pastor et al. (1990) is adopted to describe the dynamic behavior of loose sand soil under cyclic wave loading. Its reliability and applicability of this model for the problem of Fluid–Structure–Seabed-Interaction has been widely verified in Ye, J.H. (2012) and Ye et al. (2013). Taking the parameters of Neveda sand determined in the VELACS project funded by NSF as the property parameters for the loose sand bed, a small-scale computational case like the experimental set-up in Mostafa et al. (1999) is taken as a representative case to investigate the wave–structure–seabed foundation interaction mechanism. The following conclusions are made:

(1) Consolidation status of seabed foundation under marine structure and hydrostatic pressure should be determined first in computation. This consolidation status is then taken as the initial condition at $t=0$ s for the dynamic analysis of wave–seabed–structure interaction thereafter. If this consolidation status of seabed foundation is not considered, the initial stress and deformation fields in seabed foundation are all zero. Obviously, this is inappropriate. As we know, the effect of
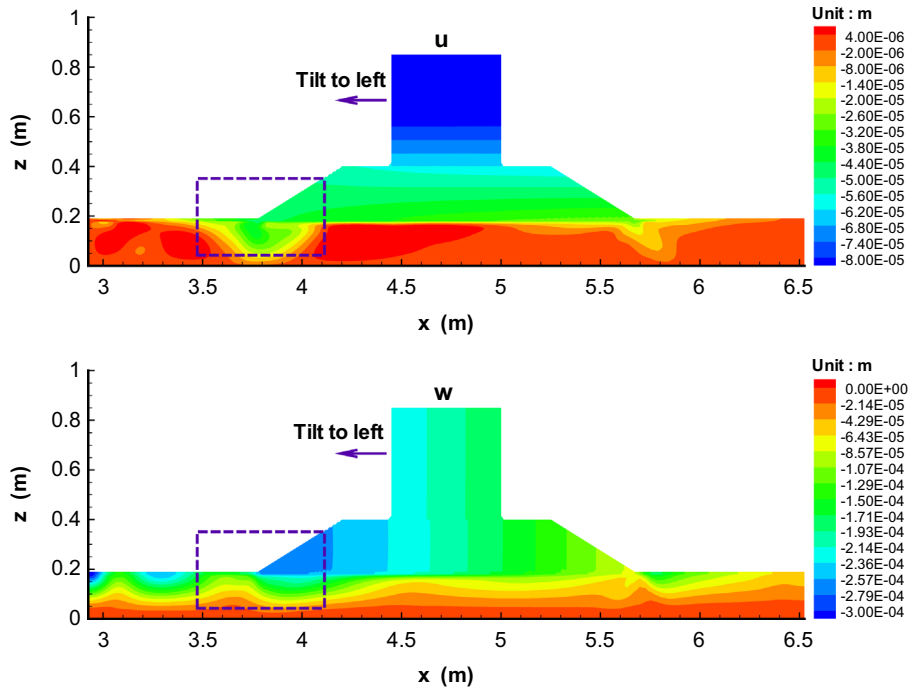
Fig. 18. Distribution of the horizontal and vertical displacement in the sandy bed and composite breakwater after time $t/T=50$.
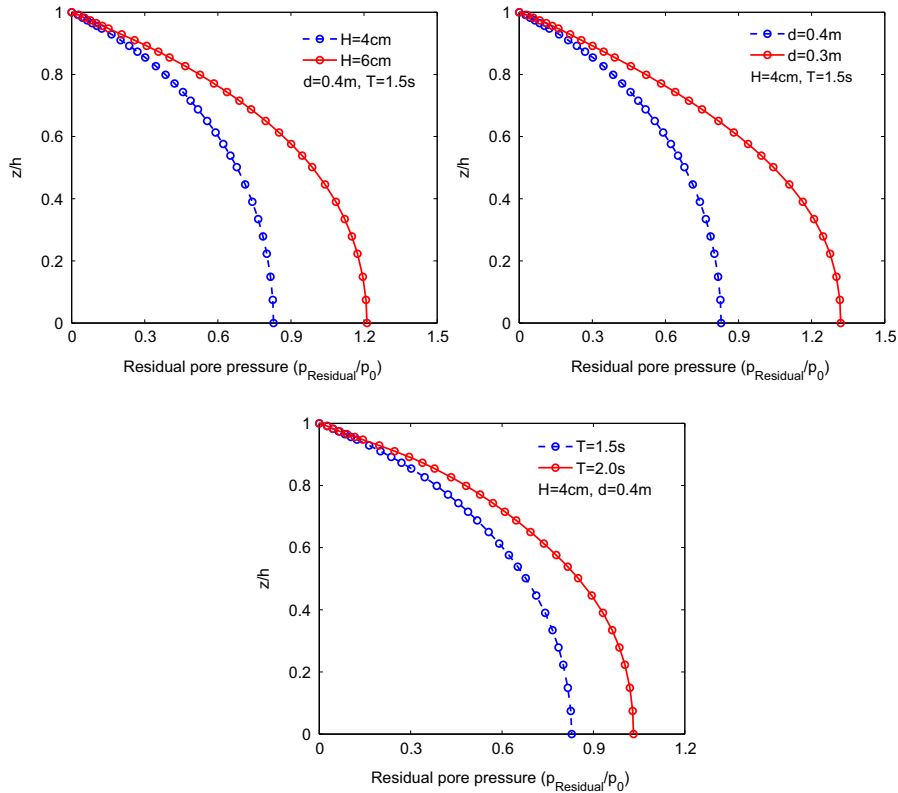

Fig. 19. Effect of wave characteristics on the wave-induced residual pore pressure in the loose sand bed at $t/T=20$ ($k = 1.0 \times 10^{-5}$ m/s, $S_r = 98\%$).

marine structures on the initial stress and deformation fields is very significant in seabed foundation.

(2) In the process of wave–seabed–structure interaction, the wave applies impact on marine structures, and applies wave-induced dynamic pressure on seabed foundation. The impact forces marine structures to vibrate correspondingly. Under the loading of wave-induced dynamic pressure on seabed, and the cyclic shearing induced by the vibration of marine structures in seabed foundation, the soil particles in loose sand soil tend to rearrange their relative position to a more denser status, and to a optical arrangement. Correspondingly, the volume contraction occurs. As a result, the pore pressure builds up; and the effective stresses vary complexly in seabed foundation. Due to the occurrence of soil compaction under wave loading for loose sand bed, marine
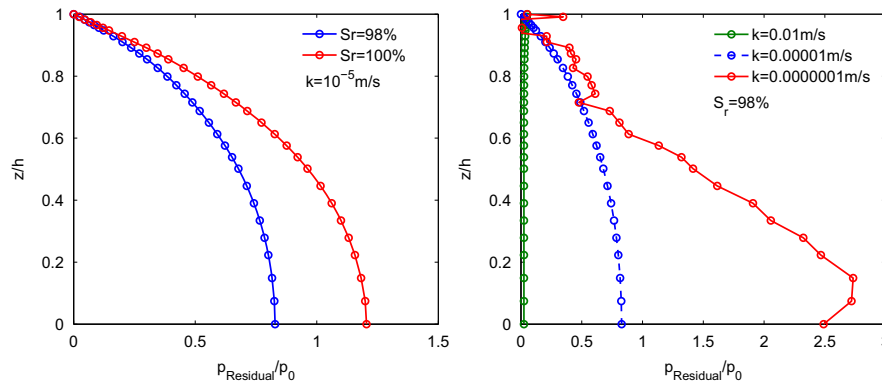
Fig. 20. Effect of soil properties on the wave-induced residual pore pressure in the loose sand bed at $t/T = 20$ ($H=6$ cm, $d=40$ cm, $T=1.5$ s).

structures built on it subside downward correspondingly. Because the magnitude of wave loading on the left and right part of seabed foundation is significantly different, the subsidence of marine structures is not uniform. As a result, marine structures built on loose sand bed would tilt to one side continuously. Once the tilt displacement excess a critical value, marine structures would collapse in the offshore environment. This could bring great economic losses, and even serious environmental pollution if the marine structure is related to oil industry.

(3) Due to the fact that the volume contraction and compaction do not occur in rubble mound comprising of large gain size gravels, the pore pressure built-up cannot occur in rubble mound. The residual pore pressure in seabed foundation increases with the time of wave loading. However, the increasing residual pore pressure at a position in seabed foundation is limited by the gravity weight of overburden soil. Although the wave loading is only applied on left side of the seabed foundation, however, the pore pressure still can built up in the right part of seabed foundation due to the pore pressure diffusion from high pressure zone to low pressure zone, and the marine structures vibration induced shearing in the sand soil under the right foot of the rubble mound.

(4) Effective stress path circles along a flat oval if the sand bed is elastic (very dense); however, the effective stress path moves substantially under wave loading for loose elasto-plastic sand bed. It is indicated that an unrecoverable interaction process occurs in the sand bed under wave loading. Stress paths in loose sand bed move fastly in the early stage; while, they move very slow in the late stage. The reason for this would be that the loose sand bed gradually becomes harder and harder under wave loading.

(5) Parametric studies show that the water waves in shallow water with larger height and longer period make the wave-induced residual pore pressure in loose seabed foundation built up more quickly; and the saturated sand bed is much easier for the residual pore pressure to built up under wave loading than the unsaturated sand bed due to the fact that the significant compressibility of pore fluids (water and trapped gas) in unsaturated sand soil. Additionally, parametric studies also indicate that the permeability of soil is the most important factor affecting the pore pressure build-up. It is impossible for pore pressure to built up in the sand soil with huge permeability due to the huge dissipation speed of pore pressure in it.

References

Cheng, L., Sumer, B.M., Fredsoe, J., 2001. Solution of pore pressure build up due to progressive waves. Int. J. Numer. Anal. Method Geomech. 25 (9), 885–907.

Choudhury, B., Dasari, G.R., Nogami, T., 2006. Laboratory study of liquefaction due to wave–seabed interaction. J. Geotech. Geoenviron. Eng. ASCE 132 (7), 842–851.

Dunn, S.L., Vun, P.L., Chan, A.H.C., Damgaard, J.S., 2006. Numerical modeling of wave-induced liquefaction around pipelines. J. Waterw., Port, Coast., Ocean Eng., ASCE 132 (4), 276–288.

Franco, L., 1994. Vertical breakwaters: the italian experience. Coast. Eng. 22 (1–2), 31–55, Special Issue Vertical Breakwaters.

Guillen, P.M., 2008. Large breakwaters in deep water in northern spain. Proc. Inst. Civil Eng., Marit. Eng. 161 (MA4), 175–186.

Harlow, H.E., 1980. Large rubble-mound breakwater failures. J. Waterw., Coast. Ocean Eng. ASCE 106 (2), 275–278.

Hsu, J.R., Jeng, D.S., 1994. Wave-induced soil response in an unsaturated anisotropic seabed of finite thickness. Int. J. Numer. Anal. Methods Geomech. 18 (11), 785–807.

Hsu, T.J., Sakakiyama, T., Liu, P.L.F., 2002. A numerical model for wave motions and turbulence flows in front of a composite breakwater. Coast. Eng. 46, 25–C50.

Jeng, D., Ye, J., 2012. Three-dimensional consolidation of a porous unsaturated seabed under rubble mound breakwater. Ocean Eng. 53, 48–59.

Jeng, D.S., Cha, D.H., Lin, Y.S., Hu, P.S., 2001. Wave-induced pore pressure around a composite breakwater. Ocean Eng. 28, 1413–1435.

Jeng, D.-S., Ye, J.H., Zhang, J.-S., Liu, P.-F., 2013. An integrated model for the wave-induced seabed response around marine structures: model, verifications and applications. Coast. Eng. 72 (1), 1–19.

Lara, J.L., Losada, I.J., Maza, M., Guanche, R., 2011. Breaking solitary wave evolution over a porous underwater step. Coast. Eng. 58 (9), 837–850.

Lee, J.F., Lan, Y.J., 2002. On waves propagating over poro-elastic infinite seabed. Ocean Eng. 29, 931–946.

Lee, T.C., Tsai, C.P., Jeng, D.S., 2002. Ocean wave propagating over a porous seabed of finite thickness. Ocean Eng. 29, 1577–1601.

Li, J., Jeng, D.S., 2008. Response of a porous seabed around breakwater heads. Ocean Eng. 35 (8–9), 864–886.

Lin, P., Karunarathna, S.A.S.A., 2007. Numerical study of solitary wave interaction with porous breakwaters. ASCE J. Waterw., Port, Coast., Ocean Eng. 133 (5), 352–363.

Lin, P., Liu, P.L.F., 1998. A numerical study of breaking waves in the surf zone. J. Fluid Mech. 359, 239–264.

Lin, Z.P., Liu, P.L.-F., 1999. Internal wave-maker for Navier–Stokes equations models. J. Waterw., Port, Coast., Ocean Eng. 99 (4), 207–215.

Liu, P.L.F., Lin, P.Z., Chang, K.A., Sakakiyama, T., 1999. Numerical modeling of wave interaction with porous structures. J. Waterw. Port, Coast., Ocean Eng., ASCE 125, 322–330.

Lu, H.B., 2005. The Research on Pore Water Pressure Response to Waves in Sandy Seabed (Ph.D. thesis). Changsha University of Science & Technology, Changsha, Hunan, China.

Lundgren, H., Lindhardt, J.H.C., Romold, C.J., 1989. Stability of breakwaters on porous foundation. In: Proceeding of 12th International Conference on Soil Mechanics and Foundation Engineering, vol. 1, pp. 451–454.

Mizutani, N., Mostarfa, A., Iwata, K., 1998. Nonliear regular wave, submerged breakwater and seabed dynamic interaction. Coast. Eng. 33, 177–202.

Mory, M., Michallet, H., Bonjean, D., Piedra-Cueva, I., Barnoud, J.M., Foray, P., Abadie, S., Breul, P., 2007. A field study of momentary liquefaction caused by waves around a coastal structure. J. Waterw., Port, Coast. Ocean Eng. ASCE 133 (1), 28–38.

Mostafa, A., Mizutani, N., Iwata, K., 1999. Nonlinear wave, composite breakwater, and seabed dynamic interaction. J. Waterw., Port, Coast., Ocean Eng. 25 (2), 88–97.

Oumeraci, H., 1994. Review and analysis of vertical breakwater failures ł lessons learned special issue on vertical breakwaters. Coast. Eng. 22, 3–29.

Pastor, M., Chan, A.H.C., Mira, P., Manzanal, D., Fernndez, M.J.A., Blanc, T., 2011. Computational geomechanics: the heritage of olek zienkiewicz. Int. J. Numer. Methods Eng. 87 (1–5), 457–489.

Pastor, M., Zienkiewicz, O.C., Chan, A.H.C., 1990. Generalized plasticity and the modelling of soil behaviour. Int. J. Numer. Anal. Methods Geomech. 14, 151–190.

Rahman, M.S., Jaber, W.Y., 1986. Simplified drained analysis for wave-induced liquefaction in ocean floor sands. Soils Found. 26 (3), 57–68.

Sassa, S., Sekiguchi, H., 1999. Wave-induced liquefaction of beds of sand in a centrifuge. Géotechnique 49 (5), 621–638.

Sassa, S., Sekiguchi, H., 2001. Analysis of wave-induced liquefaction of sand beds. Géotechnique 51 (2), 115–126.

Sassa, S., Sekiguchi, H., Miyamoto, J., 2001. Analysis of progressive liquefaction as a moving-boundary problem. Géotechnique 51 (10), 847–857.

Sassa, S., Takayama, T., Mizutani, M., Tsujio, D., 2006. Field observations of the build-up and dissipation of residual porewater pressures in seabed sands under the passage of stormwaves. J. Coast. Res. 39, 410–414.

Silvester, R., Hsu, J.R.C., 1989. Sines revisited. J. Waterw., Port, Coast., Ocean Eng., ASCE 115 (3), 327–344.

Sorenson, T., 1992. Breakwater failure brings lessons (ltr). Civil Eng.—ASCE 62 (9), 37–38.

Sumer, B.M., Kirca, V.S.O., Fredsoe, J., 2011. Experimental validation of a mathematical model for seabed liquefaction in waves. In Proceedings of the International Offshore and Polar Engineering Conference, pp. 1010–1018.

Sumer, M.B., Dixen, F.H., Fredsoe, J., 2010. Cover stones on liquefiable soil bed under waves. Coast. Eng. 57 (9), 864–873.

Teh, T.C., Palmer, A.C., Damgaard, J.S., 2003. Experimental study of marine pipeline on unstable and liquefied seabed. Coast. Eng. 50 (1–2), 1–17.

Tsai, C.P., Lee, T.L., 1995. Standing wave induced pore pressure in a porous seabed. Ocean Eng. 22 (6), 505–517.

Tzang, S.-Y., Chen, Y.L., Ou, S.-H., 2011. Experimental investigations on developments of velocity field near above a sandy bed during regular wave-induced fluidized responses. Ocean Eng. 38 (7), 868–877.

Ulker, M.B.C., Rahman, M.S., Guddati, M.N., 2010. Wave-induced dynamic response and instability of seabed around caisson breakwater. Ocean Eng. 37 (17–18), 1522–1545.

Ye, J., 2012a. 3D liquefaction criteria for seabed considering the cohesion and friction of soil. Appl. Ocean Res. 37, 111–119.

Ye, J., 2012b. Numerical modelling of consolidation of 2-D porous unsaturated seabed under a composite breakwater. Mechanika 18 (4), 373–379.

Ye, J., Jeng, D., Chan, A., 2012. Consolidation and dynamics of 3D unsaturated porous seabed under rigid caisson breakwater loaded by hydrostatic pressure and wave. Sci. China Technol. Sci. 55 (8), 2362–2376.

Ye, J., Jeng, D.-S., Wang, R., Zhu, Z.-Q., 2013. Validation of a 2D semi-coupled numerical model for fluid-structures-seabed interaction. J. Fluids Struct. 42, 333–357.

Ye, J.H., 2012. Numerical Analysis of Wave–Seabed–Breakwater Interactions (Ph.D. thesis). University of Dundee, Dundee, UK.

Zen, K., Umehara, Y., Finn, W.D.L., 1985. A case study of the wave-induced liquefaction of sand layers under damaged breakwater. In: Proceeding 3rd Canadian Conference on Marine Geotechnical Engineering, Canada, pp. 505–520.

Zen, K., Yamazaki, H., 1990. Oscillatory pore pressure and liquefaction in seabed induced by ocean waves. Soils Found. 30 (4), 147–161.

Zhang, F.G., Ge, Z.J., 1996. A study on some causes of rubble mound breakwater failure. China Ocean Eng. 10 (4), 473–481.

Zhou, X.-L., Xu, B., Wang, J.-H., Li, Y.-L., 2011. An analytical solution for wave-induced seabed response in a multi-layered poro-elastic seabed. Ocean Eng. 38 (1), 119–129.

Zienkiewicz, O.C., Chan, A.H.C., Pastor, M., Schrefler, B.A., Shiomi, T., 1999. Computational Geomechanics with Special Reference to Earthquake Engineering. John Wiley and Sons, England.

Zienkiewicz, O.C., Chang, C.T., Bettess, P., 1980. Drained, undrained, consolidating and dynamic behaviour assumptions in soils. Geotechnique 30 (4), 385–395.